

**A comparison of global heat flow interpolation
techniques**

Buchanan C. Kerswell¹Matthew J. Kohn¹

¹Department of Geosciences, Boise State University, Boise, ID 83725

Key Points:

-
-
-

9 **Abstract**

10 **1 Introduction**

11 Heat escaping the solid Earth's surface indicates a dynamically cooling planet. Surface heat flow databases (Hasterok & Chapman, 2008; Luazeau, 2019; Pollack et al., 1993) provide a way to understand geodynamics by relating the amount of heat escaping Earth's surface to heat-transferring and heat-generating subsurface processes such as diffusion, hydrothermal circulation, radioactive decay, fault motion, subduction dynamics, and mantle convection (Currie et al., 2004; Currie & Hyndman, 2006; Fourier, 1827; Furlong & Chapman, 2013; Furukawa, 1993; Gao & Wang, 2014; Hasterok, 2013; Kerswell et al., 2020; Parsons & Sclater, 1977; Pollack & Chapman, 1977; Rudnick et al., 1998; Stein & Stein, 1992, 1994; Wada & Wang, 2009). Surface heat flow observations continue to motivate research, evident by more than 1,393 publications compiled in the most recent heat flow dataset, although the rate of publications using surface heat flow has declined since the mid 1980's (Jennings & Hasterok, 2021).

23 Many research questions, such as calculating the global surface heat flux from continents and oceans, require interpolating discrete heat flow observations onto a continuous approximation of Earth's surface. Previous attempts at interpolation use one or more geographic, geologic, geochronologic, or geophysical proxies to predict heat flow at unknown locations by association with similar observation sites (e.g., bathymetry or elevation, proximity to active or ancient orogens, seafloor age, upper mantle shear wave velocities, Chapman & Pollack, 1975; Davies, 2013; Goutorbe et al., 2011; Lee & Uyeda, 1965; Luazeau, 2019; Sclater & Francheteau, 1970; Shapiro & Ritzwoller, 2004). These methods are called *similarity methods* (Figure 1). The success of such interpolations are typically evaluated statistically by the misfit between the predicted and observed heat flow. However, even statistically-successful heat flow interpolations are difficult to interpret and show unexpected anomalies (Luazeau, 2019). The fidelity and usefulness of interpolations depend on the question being asked and the choice of methodology.

36 Predicting surface heat flow by association with physical proxies is arguably the most reasonable approach to interpolation for global investigations. Our understanding of geodynamics and near-surface heat flow perturbations implies that the variance in surface heat flow is not uniformly stochastic, but rather, in large part, determined by the

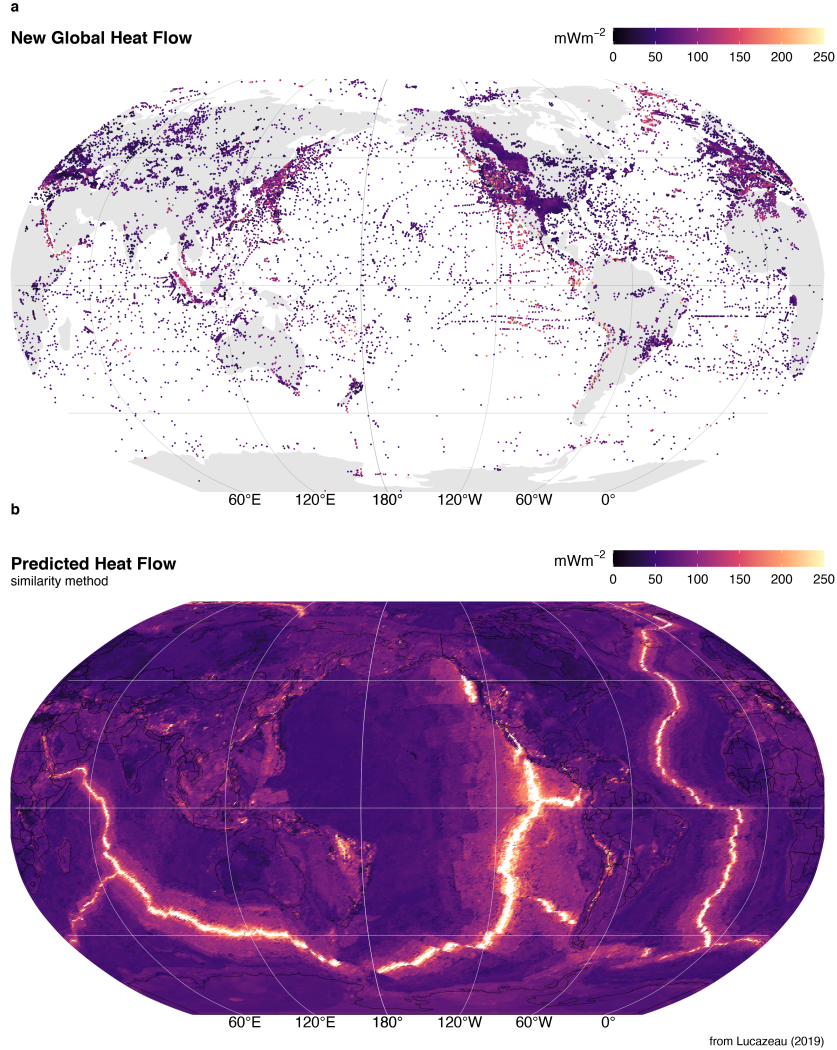


Figure 1: The NGHF dataset. (a) The complete dataset ($n = 69729$), and (b) interpolation by similarity method from Lucaleau (2019).

physical conditions and processes operating locally (e.g., Goutorbe et al., 2011). For example, younger oceanic plates should have higher surface heat flow than older plates (Stein & Stein, 1992), subducting oceanic plates will lower surface heat flow near trenches (Fukukawa, 1993), and hydrothermal circulation of seawater can modify heat flow in oceanic crust (Hasterok et al., 2011). Interpolation by association with physical proxies makes reasoned predictions of heat flow based on many independently-tested geodynamic models. However, similarity methods are strongly biased towards such models and risk making determinations where, in fact, surprising results and idiosyncrasies may be found.

48 In contrast, there exists some degree of stationarity, spatial dependence, or con-
49 tinuity, in the distribution of surface heat flow. A pair of surface heat flow observations
50 taken one meter apart will be strongly correlated. The correlation between pairs of ob-
51 servations will likely decrease with increasing distance between the pairs (Goovaerts, 1997).
52 The spatial (dis)continuity of surface heat flow represents the areal extent of geodynamic
53 processes and their interactions. For example, consistent patterns of heat flow near vol-
54 canic arcs are interpreted to reflect common backarc lithospheric thermal structures and
55 slab-mantle mechanical coupling depths in subduction zones (Furukawa, 1993; Kerswell
56 et al., 2020; Wada & Wang, 2009).

57 In theory, one may predict surface heat flow at unknown locations by considering
58 many nearby observations (i.e. Kriging, Krige, 1951). However, Kriging is disadvanta-
59 geous for global interpolations of surface heat flow because it assumes that the under-
60 lying distribution of heat flow is stationary (constant in space), which effectively ignores
61 geodynamic complexity. One can overcome this problem by relaxing assumptions of sta-
62 tionarity, or applying Markov-Bayes techniques to include proxies as priors (Bárdossy,
63 1997). Instead, we leverage the properties of stationarity as a tool for comparison with
64 *similarity* methods of interpolation (Goutorbe et al., 2011; Lucaleau, 2019). So the ques-
65 tions are: 1) What are the differences between Kriging and similarity methods? 2) What
66 are the implications of the differences according to the implicit assumptions in both meth-
67 ods?

68 We attempt to answer these questions by using ordinary Kriging to interpolate the
69 New Global Heat Flow (NGHF) dataset of Lucaleau (2019). Our method is optimized
70 using a genetic algorithm to minimize an objective function which considers both the
71 misfit on the variogram models and interpolation results (after Li et al., 2018). We then
72 compare our interpolation results to those of Lucaleau (2019) and consider the impli-
73 cations of Kriging vs. similarity methods of interpolation. We restrict our comparison
74 to areas near subduction zone segments defined by Syracuse & Abers (2006) for two rea-
75 sons: 1) to provide maps and statistics useful to subduction zone research, and 2) to em-
76 phasize differences and idiosyncrasies in both interpolation approaches in a complex tec-
77 tonic and thermal setting.

78 **2 Methods**

79 **2.1 The NGHF Dataset**

80 The NGHF dataset was downloaded from the supplementary material of Lucaleau
 81 (2019). It contains 69729 data points, their locations in latitude/longitude, and metadata—
 82 including a data quality rank (Code 6) from A to D (with Code 6 = Z = undetermined).
 83 The reader is referred to Lucaleau (2019) for details on compilation, references, and his-
 84 torical perspective on the NGHF and previous compilations. We use NGFH because it
 85 is the most recent dataset available, has been carefully compiled, and is open-access.

86 Like Lucaleau (2019), we exclude 4790 poor quality observations (Code 6 = D) from
 87 our analysis. We further remove 350 data points without heat flow observations and two
 88 without geographic information. Multiple observations at the same location are parsed
 89 to avoid singular covariance matrices during Kriging:

$$\begin{aligned}
 f(X_i^q, Y_i^q) = & \\
 X_i^q > Y_i^q \rightarrow z_i &= x_i \\
 X_i^q < Y_i^q \rightarrow z_i &= y_i \\
 X_i^q = Y_i^q \rightarrow z_i &= RAND(x_i, y_i)
 \end{aligned} \tag{1}$$

90 where X_i^q and Y_i^q represent the quality of each duplicate observation pair at loca-
 91 tion i , $RAND$ is a random function that selects either the observation x_i or y_i , and z_i
 92 stores the observation selected by $f(X_i^q, Y_i^q)$. The final dataset used for Kriging has $n =$
 93 55274 observations after parsing $n = 32430$ duplicate observation.

94 **2.2 Kriging**

95 Kriging is a three-step process that involves first estimating an experimental vari-
 96 iogram, $\hat{\gamma}(h)$, fitting the experimental variogram with one of many variogram models,
 97 $\gamma(h)$, and finally using the modelled variogram to predict random variables at unknown
 98 locations (Cressie, 2015; Krige, 1951). We use the general-purpose functions defined in
 99 the “R” package `gstat` (Gräler et al., 2016; Pebesma, 2004) to perform all three steps.
 100 We begin by estimating an experimental variogram as defined by Bárdossy (1997):

$$\hat{\gamma}(h) = \frac{1}{2N(h)} \sum_{N(h)} (Z(u_i) - Z(u_j))^2 \quad (2)$$

where $N(h)$ is the number of pairs of points, $Z(u_i)$ and $Z(u_j)$, separated by a lag distance, $h = |u_i - u_j|$. We evaluate $\hat{\gamma}(h)$ at fifteen lag distances by binning the irregular spaced data with a bin width, δ , equal to one-third of the maximum lag distance divided by the number of lags used to evaluate the variogram, $\delta = \max(N(h))/(3 \cdot 15)$. Then $N(h) \leftarrow N(h, \delta h) = \{i, j : |u_i - u_j| \in [h - \delta h, h + \delta h]\}$. In simple terms, Equation 2 represents the similarity, or dissimilarity, between pairs of observations in space. Equation 2 is derived from the theory of *regionalized variables* (Matheron, 1963, 2019), which formally defines a probabilistic framework for spatial interpolation of natural phenomena. It is important for the reader to understand the fundamental assumptions implicit in Equation 2 in order to understand the comparison of interpolation techniques discussed later. The basic assumptions used in our Kriging method are:

- $\hat{\gamma}(h)$ is directionally invariant (isotropic)
- $\hat{\gamma}(h)$ is evaluated in two-dimensions and neglects elevation, $Z(u) \in \mathbb{R}^2$
- The first and second moments of $Z(u)$ have the following conditions over the domain D :

$$\begin{aligned} E[Z(u)] &= \text{mean} = \text{constant}, & \forall u \in D \\ E[(Z(u + h) - \text{mean})(Z(u) - \text{mean})] &= C(h), & \forall |u, u + h| \in D \end{aligned} \quad (3)$$

The last assumption (Equation 3) is called “second-order stationarity” and is commonly used in practice. It assumes the underlying probability distribution of the random variable, $Z(u)$, does not change in space and the covariance, $C(h)$, only depends on the distance, h , between two random variables. These assumptions are expected to be valid in cases where the underlying natural process is stochastic, spatially continuous, and has the property of additivity such that $\frac{1}{n} \sum_{i=1}^n Z(u_i)$ has the same meaning as $Z(u)$ (Bárdossy, 1997).

The following are two illustrative cases where Equation 3 is likely valid:

1. The thickness of a sedimentary unit with a homogeneous concentration of radioactive elements can be approximated by $q_s = q_b + \int A dz$, where q_b is a constant heat flux entering the bottom of the layer and A is the heat production within the

layer with thickness z (Furlong & Chapman, 2013). If we have two samples, $Z(u_1) = 31 \text{ mW/m}^2$ and $Z(u_2) = 30.5 \text{ mW/m}^2$, their corresponding thicknesses would be $Z'(u_1) = 1000 \text{ m}$ and $Z'(u_2) = 500 \text{ m}$ for $A = 0.001 \text{ mW/m}^3$ and $q_b = 30 \text{ mW/m}^2$. The variable, $Z(u)$, in this case is additive because the arithmetic mean of the samples is a good approximation of the average sedimentary layer thickness, $(Z(u_1) + Z(u_2))/2 = 750 \text{ m}$.

- 127
 - 128
 - 129
 - 130
 - 131
 - 132
 - 133
 - 134
 - 135
 - 136
 - 137
 - 138
 - 139
 - 140
 - 141
 - 142
 - 143
 - 144
 - 145
 - 146
 - 147
 - 148
 - 149
 - 150
 - 151
 - 152
 - 153
 - 154
2. The age of young oceanic lithosphere can be approximated by $q_s(t) = kT_b(\pi\kappa t)^{-1/2}$, where $q_s(t)$ is the surface heat flow of a plate with age, t , T_b is the temperature at the base of the plate, k is thermal conductivity, and $\kappa = k/\rho C_p$ is thermal diffusivity (Stein & Stein, 1992). For $k = 3.138 \text{ W/mK}$, $\rho = 3330 \text{ kg/m}^3$, $C_p = 1171 \text{ J/kgK}$, $T_b = 1350^\circ\text{C}$, two samples, $Z(u_1) = 180 \text{ mW/m}^2$ and $Z(u_2) = 190 \text{ mW/m}^2$, would correspond to plates with ages of $Z'(u_1) = 10 \text{ Ma}$, and $Z'(u_2) = 9 \text{ Ma}$, respectively. Since $Z(u_1)+Z(u_2)/2 = 185 \text{ mW/m}^2$ and $Z'(185 \text{ mW/m}^2) = 9.5 \text{ Ma} = Z'(u_1) + Z'(u_2)/2$, the variable $Z(u)$ in this case is also additive.

In contrast, Equation 3 is likely invalid in regions that transition among two or more tectonic regimes. For example, the expected heat flow $E[Z(u)] = \text{mean}$ will change when moving from a spreading center to a subduction zone. $E[Z(u)] = \text{mean} \neq \text{constant}$ over the region of interest. Proceeding with Equation 3 in this case has the effect of masking the geodynamic complexity. In other words, the spatial dependence is considered in the Kriging method in this case, but the geodynamic structure is *invisible*. We will see that this has important implications when comparing our Kriging method to Lucaleau (2019)'s interpolation method, which is exactly opposite of this formalism—it only considers the similarities among physical proxies and not spatial dependence.

The second step is to fit the experimental variogram with a variogram model, $\gamma(h)$. In this study we fit three popular variogram models to the experimental variogram. We use models with sill, which implies the spatial dependence between pairs of points has a finite range. The spherical, exponential, and Gaussian variogram models are defined as (Chiles & Delfiner, 2009; Cressie, 2015):

$$\begin{aligned}
sph \leftarrow \gamma(h) &= \begin{cases} n + s \left(\frac{3h}{2a} - \frac{1}{2} \left(\frac{h}{a} \right)^3 \right), & \text{if } 0 \leq h \leq a \\ n + s, & \text{if } h > a \end{cases} \\
exp \leftarrow \gamma(h) &= n + s \left(1 - \exp \left(\frac{-h}{a} \right) \right), \quad \text{if } h \geq 0 \\
Gau \leftarrow \gamma(h) &= n + s \left(1 - \exp \left(\frac{-h^2}{a^2} \right) \right), \quad \text{if } h \geq 0
\end{aligned} \tag{4}$$

where n is the nugget, s is the sill, and a is the effective range. For spherical, exponential, and Gaussian models, the effective range is related to the range, r , by $a = r$, $a = r/3$, and $a = 1/r\sqrt{3}$, respectively (Gräler et al., 2016; Pebesma, 2004). The function `fit.variogram` in `gstat` allows one to try many variogram models and the best will be selected by the minimum misfit by weighted least square (WLS, Pebesma, 2004).

We use ordinary Kriging for our interpolation step, which predicts the value of a random function, $\hat{Z}(u)$ at unknown locations as a linear combination of all known locations in the domain, D (Bárdossy, 1997):

$$\hat{Z}(u) = \sum_{i=1}^n \lambda_i Z(u_i), \quad \forall u \in D \tag{5}$$

The conditions in Equation 3 set up a constrained minimization problem since one has:

$$E[Z(u)] = mean, \quad \forall u \in D \tag{6}$$

The linear estimator must obey

$$E[\hat{Z}(u)] = \sum_{i=1}^n \lambda_i E[Z(u_i)] = mean \tag{7}$$

so the weights must be:

$$\sum_{i=1}^n \lambda_i = 1 \tag{8}$$

This is the first constraint, also known as the unbiased condition, which states that the sum of the weights must equal one. However, there is an infinite set of real numbers

one could use for the weights, λ_i . Our goal is to find the set of weights in Equation 5 that minimizes the estimation variance. This can be solved with the covariance function, $C(h)$ from Equation 3:

$$\begin{aligned}\sigma^2(u) &= \text{Var}[Z(u) - \hat{Z}(u)] = E \left[(Z(u) - \sum_{i=1}^n \lambda_i Z(u_i))^2 \right] = \\ &E \left[Z(u)^2 + \sum_{j=1}^n \sum_{i=1}^n \lambda_j \lambda_i Z(u_j) Z(u_i) - 2 \sum_{i=1}^n \lambda_i Z(u_i) Z(u) \right] = \\ &C(0) + \sum_{j=1}^n \sum_{i=1}^n \lambda_j \lambda_i C(u_i - u_j) - 2 \sum_{i=1}^n \lambda_i C(u_i - u)\end{aligned}\quad (9)$$

Solving for the weights in Equation 5 with respect to the unbiased condition (Equation 8) and minimum estimate variance (Equation 9), yields the best linear unbiased estimator (BLUE, Bárdossy, 1997). In our case, this is done by the function `krige` in `gstat`.

2.3 Kriging Optimization

Achieving a useful Kriging results depends on one's choice of many Kriging parameters (Θ). In this study, we investigate a set of parameters, Θ :

$$\Theta = \{m, s, a, n, S\} \quad (10)$$

where m is the model type (sph, exp, or Gau), s is the sill, a is the effective range, n is the nugget, and S is the maximum distance for local Kriging. Only points within S from the prediction location are used for Kriging. Our goal is to find Θ such that our interpolation, $f(x_i; \Theta)$, gives the most useful outcome—defined by minimizing a cost function, $C(\Theta)$, that represents the error between the set of real observations, $Z(u_i)$ and predictions, $\hat{Z}(u)$.

We define a cost function that simultaneously considers the misfit between the experimental and modelled variogram and between the Kriging predictions and observed heat flow (after Li et al., 2018):

$$C(\Theta) = (1 - w)C_F(\Theta) + wC_I(\Theta) \quad (11)$$

187 where $C_F(\Theta)$ is the root mean square error (RMSE) of the modelled variogram fit
 188 calculated by WLS, and $C_I(\Theta)$ is the RMSE of the Kriging result calculated by cross-
 189 validation. The weight, w , is set to 0.5 in our study, which balances the effects of $C_F(\Theta)$
 190 and $C_I(\Theta)$ on the cost function. The final expression to minimize becomes:

$$\min(C(\Theta)) = \frac{1-w}{\sigma_E} \sqrt{\frac{1}{N} \sum_{k=1}^N w(h_k)[\hat{\gamma}(h_k) - \gamma(h_k; \Theta)]^2} + \frac{w}{\sigma_S} \sqrt{\frac{1}{M} \sum_{i=1}^M [Z(u_i) - \hat{Z}(u_i; \Theta)]^2} \quad (12)$$

191 where N is the number of pairs of points used to calculate the experimental var-
 192 iogram, $\hat{\gamma}(h_k)$, σ_E is the standard deviation of the experimental variogram, $\hat{\gamma}(h)$, $w(h_k)$
 193 is the weight in WLS and defines the importance of the k th lag in the error estimate.
 194 We use $w(h_k) = N_k/h_k^2$. $Z(u_i)$ and $\hat{Z}(u_i; \Theta)$ are the measured and predicted values,
 195 respectively, σ_s is the standard deviation of the predicted values, $\hat{Z}(u_i)$, and M is the
 196 number of measurements in $Z(u_i)$. For $C_I(\Theta)$ we use ten-fold cross-validation, which splits
 197 the dataset, $|Z(u_i), \forall u_i \in D|$ into ten equal intervals and tests one interval against the
 198 remaining nine. This process is then repeated over all intervals so that the whole dataset
 199 has been cross-validated.

200 Minimization of $C(\Theta)$ is achieved by a genetic algorithm that simulates biologic
 201 natural selection by differential success (Goldberg, 1989). Our procedure is as follows:

- 202 1. Initiate fifty *chromosomes*, ξ , with random starting parameters defined within the
 203 search domain (Table 1)
- 204 2. Evaluate the fitness of each individual chromosome as $-C(\Theta)$ for the entire pop-
 205 ulation
- 206 3. Allow the population to exchange genetic information by sequentially performing
 207 genetic operations:
 - 208 a. Selection: the top 5% fittest chromosomes survive each generation
 - 209 b. Crossover: pairs of chromosomes have an 80% chance of exchanging genetic in-
 210 formation
 - 211 c. Mutation: there is a 10% chance for random genetic mutations
- 212 4. Evaluate the fitness of the new population

- 213 5. If the termination criterion is met, do step (6), otherwise continue to evolve by
 214 repeating steps (3) and (4)
 215 6. Decode the best chromosome and build the optimal variogram

216 We use the general-purpose functions in the “R” package **GA** (Scrucca, 2013, 2016)
 217 to perform each step in the above procedure.

Table 1: Parameters and ranges used in the optimization algorithm

Parameter	Search Domain	Units
Model (m)	[Spherical, Exponential, Guassian]	NA
Sill (s)	[1, 5×10^3]	$(mW/m^2)^2$
Effective Range (a)	[1, 1×10^6]	meters
Nugget (n)	[1, 1×10^3]	meters
Local Search (S)	[1, 1×10^6]	meters

218 2.4 Map Projection and Interpolation Grid

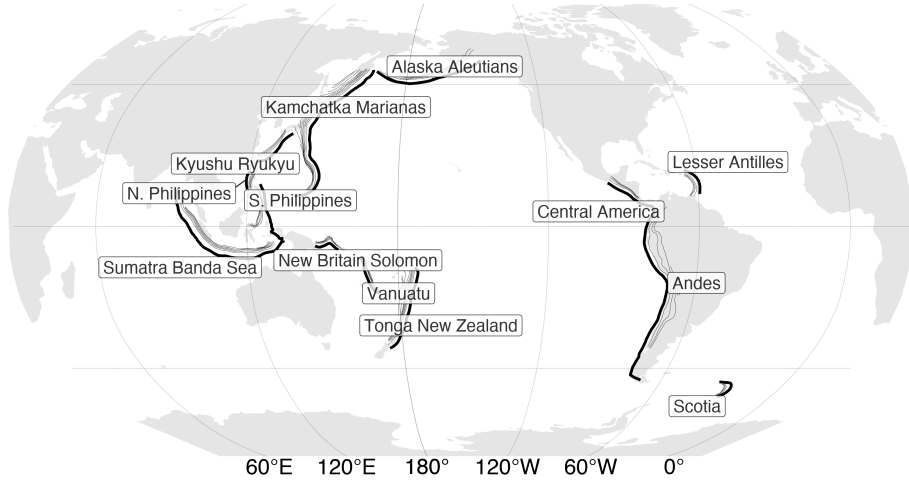
219 We interpolate onto the same $0.5^\circ\text{C} \times 0.5^\circ\text{C}$ grid as Luazeau (2019) so a direct
 220 difference could be calculated between our interpolation methods and Luazeau (2019)’s.
 221 The NGHF and grid with predicted heat flow from Luazeau (2019) were transformed
 222 into a Pacific-centered Robinson coordinate reference system (CRS) defined using the
 223 proj string (PROJ contributors, 2021):

```
224 +proj=robin +lon_0=-155 +lon_wrap=-155 +x_0=0 +y_0=0
225 +ellps=WGS84 +datum=WGS84 +units=m +no_defs
```

226 All geographic operations, including Kriging, are performed in the above CRS us-
 227 ing the general-purpose functions in the “R” package **sf** (Pebesma, 2018). We define the
 228 Kriging domain near individual arc segments in two steps: 1) 1000 km buffers are drawn
 229 around the arc segments as defined by Syracuse & Abers (2006). 2) The bounding box
 230 of the 1000 km buffer is expanded by 10% on all sides (Figure 2). We provide the com-
 231 plete NGHF dataset (Luazeau, 2019), filtered and parsed NGHF dataset, heat flow in-
 232 terpolations (from Luazeau, 2019, and this study), and our code as supplementary in-

233 formation to support FAIR data policy (Wilkinson et al., 2016). These items can also
234 be retrieved from the official repository at <https://doi.org/10.17605/OSF.IO/CA6ZU>.

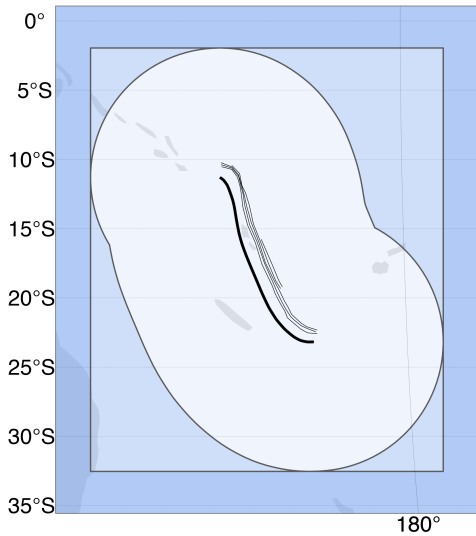
a Subduction Zone Segments



from Syracuse & Abers (2006)

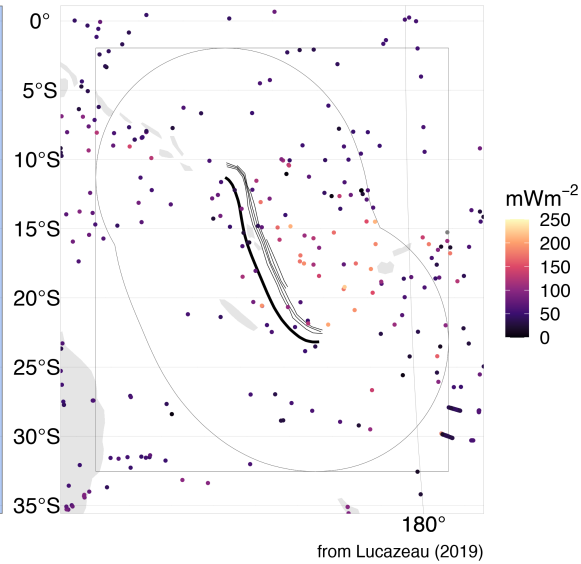
b Vanuatu

Interpolation Domain



c Vanuatu

n = 349



from Lucazeau (2019)

Figure 2: Subduction zone segments and interpolation domain. (a) Heat flow is interpolated around thirteen subduction zone segments by (b) drawing a 1000km buffer (lightest blue) around each segment and expanding the buffer's bounding box (medium blue) by 10% on all sides (darkest blue). (c) The NGHF dataset is cropped within the largest rectangle. Data from Syracuse & Abers (2006) and Lucazeau (2019).

235 **3 Results**

236 **4 Discussion**

237 **5 Conclusions**

238 **Acknowledgments**

239 **References**

- 240 Bárdossy, A. (1997). Introduction to geostatistics. *Institute of Hydraulic Engineering,*
 241 *University of Stuttgart.*
- 242 Chapman, D. S., & Pollack, H. N. (1975). Global heat flow: A new look. *Earth and Plan-*
 243 *etary Science Letters, 28*(1), 23–32.
- 244 Chiles, J.-P., & Delfiner, P. (2009). *Geostatistics: Modeling spatial uncertainty* (Vol. 497).
 245 John Wiley & Sons.
- 246 Cressie, N. (2015). *Statistics for spatial data*. John Wiley & Sons.
- 247 Currie, C., & Hyndman, R. D. (2006). The thermal structure of subduction zone back
 248 arcs. *Journal of Geophysical Research: Solid Earth, 111*(B8).
- 249 Currie, C., Wang, K., Hyndman, R. D., & He, J. (2004). The thermal effects of steady-
 250 state slab-driven mantle flow above a subducting plate: The Cascadia subduction zone
 251 and backarc. *Earth and Planetary Science Letters, 223*(1-2), 35–48.
- 252 Davies, J. H. (2013). Global map of solid earth surface heat flow. *Geochemistry, Geo-*
 253 *physics, Geosystems, 14*(10), 4608–4622.
- 254 Fourier, J. (1827). Mémoire sur les températures du globe terrestre et des espaces planétaires.
 255 *Mémoires de l'Académie Royale Des Sciences de l'Institut de France, 7*, 570–604.
- 256 Furlong, K. P., & Chapman, D. S. (2013). Heat flow, heat generation, and the thermal
 257 state of the lithosphere. *Annual Review of Earth and Planetary Sciences, 41*, 385–
 258 410.
- 259 Furukawa, Y. (1993). Depth of the decoupling plate interface and thermal structure un-
 260 der arcs. *Journal of Geophysical Research: Solid Earth, 98*(B11), 20005–20013.
- 261 Gao, X., & Wang, K. (2014). Strength of stick-slip and creeping subduction megathrusts
 262 from heat flow observations. *Science, 345*(6200), 1038–1041.
- 263 Goldberg, D. E. (1989). Genetic algorithms in search. *Optimization, and MachineLearn-*
 264 *ing.*
- 265 Goovaerts, P. (1997). *Geostatistics for natural resources evaluation*. Oxford University
 266 Press on Demand.

- 267 Goutorbe, B., Poort, J., Lucaleau, F., & Raillard, S. (2011). Global heat flow trends re-
268 solved from multiple geological and geophysical proxies. *Geophysical Journal International*, 187(3), 1405–1419.
- 270 Gräler, B., Pebesma, E., & Heuvelink, G. (2016). Spatio-temporal interpolation using
271 gstat. *The R Journal*, 8, 204–218. Retrieved from <https://journal.r-project.org/archive/2016/RJ-2016-014/index.html>
- 273 Hasterok, D. (2013). A heat flow based cooling model for tectonic plates. *Earth and Plan-
274 etary Science Letters*, 361, 34–43.
- 275 Hasterok, D., & Chapman, D. (2008). Global heat flow: A new database and a new ap-
276 proach. In *AGU fall meeting abstracts* (Vol. 2008, pp. T21C–1985).
- 277 Hasterok, D., Chapman, D., & Davis, E. (2011). Oceanic heat flow: Implications for global
278 heat loss. *Earth and Planetary Science Letters*, 311(3-4), 386–395.
- 279 Jennings, S., & Hasterok, D. (2021). HeatFlow.org. *Heatflow.org*. Retrieved from <http://heatflow.org/>
- 281 Kerswell, B. C., Kohn, M. J., & Gerya, T. V. (2020). Backarc lithospheric thickness and
282 serpentine stability control slab-mantle coupling depths in subduction zones. *Earth
283 and Space Science Open Archive*, 34. [https://doi.org/10.1002/essoar.10503710
284 .1](https://doi.org/10.1002/essoar.10503710.1)
- 285 Krige, D. G. (1951). A statistical approach to some basic mine valuation problems on
286 the witwatersrand. *Journal of the Southern African Institute of Mining and Metal-
287 lurgy*, 52(6), 119–139.
- 288 Lee, W. H., & Uyeda, S. (1965). Review of heat flow data. *Terrestrial Heat Flow*, 8, 87–
289 190.
- 290 Li, Z., Zhang, X., Clarke, K. C., Liu, G., & Zhu, R. (2018). An automatic variogram mod-
291 eling method with high reliability fitness and estimates. *Computers & Geosciences*,
292 120, 48–59.
- 293 Lucaleau, F. (2019). Analysis and mapping of an updated terrestrial heat flow data set.
294 *Geochemistry, Geophysics, Geosystems*, 20(8), 4001–4024.
- 295 Matheron, G. (1963). Principles of geostatistics. *Economic Geology*, 58(8), 1246–1266.

- 296 Matheron, G. (2019). *Matheron's theory of regionalized variables*. International Asso-
297 ciation for.
- 298 Parsons, B., & Sclater, J. G. (1977). An analysis of the variation of ocean floor bathymetry
299 and heat flow with age. *Journal of Geophysical Research*, 82(5), 803–827.
- 300 Pebesma, E. (2004). Multivariable geostatistics in S: The gstat package. *Computers &*
301 *Geosciences*, 30, 683–691.
- 302 Pebesma, E. (2018). Simple Features for R: Standardized Support for Spatial Vector Data.
303 *The R Journal*, 10(1), 439–446. <https://doi.org/10.32614/RJ-2018-009>
- 304 Pollack, H. N., & Chapman, D. S. (1977). On the regional variation of heat flow, geotherms,
305 and lithospheric thickness. *Tectonophysics*, 38(3-4), 279–296.
- 306 Pollack, H. N., Hurter, S. J., & Johnson, J. R. (1993). Heat flow from the earth's inte-
307 rior: Analysis of the global data set. *Reviews of Geophysics*, 31(3), 267–280.
- 308 PROJ contributors. (2021). *PROJ coordinate transformation software library*. Open Source
309 Geospatial Foundation. Retrieved from <https://proj.org/>
- 310 Rudnick, R. L., McDonough, W. F., & O'Connell, R. J. (1998). Thermal structure, thick-
311 ness and composition of continental lithosphere. *Chemical Geology*, 145(3-4), 395–
312 411.
- 313 Sclater, J. G., & Francheteau, J. (1970). The implications of terrestrial heat flow obser-
314 vations on current tectonic and geochemical models of the crust and upper mantle
315 of the earth. *Geophysical Journal International*, 20(5), 509–542.
- 316 Scrucca, L. (2013). GA: A package for genetic algorithms in r. *Journal of Statistical Soft-
317 ware*, 53(4), 1–37.
- 318 Scrucca, L. (2016). On some extensions to GA package: Hybrid optimisation, parallelisi-
319 sation and islands evolution. *arXiv Preprint arXiv:1605.01931*.
- 320 Shapiro, N. M., & Ritzwoller, M. H. (2004). Inferring surface heat flux distributions guided
321 by a global seismic model: Particular application to antarctica. *Earth and Planetary
322 Science Letters*, 223(1-2), 213–224.
- 323 Stein, C. A., & Stein, S. (1992). A model for the global variation in oceanic depth and
324 heat flow with lithospheric age. *Nature*, 359(6391), 123–129.

- 325 Stein, C. A., & Stein, S. (1994). Constraints on hydrothermal heat flux through the oceanic
326 lithosphere from global heat flow. *Journal of Geophysical Research: Solid Earth*, 99(B2),
327 3081–3095.
- 328 Syracuse, E. M., & Abers, G. A. (2006). Global compilation of variations in slab depth
329 beneath arc volcanoes and implications. *Geochemistry, Geophysics, Geosystems*, 7(5).
- 330 Wada, I., & Wang, K. (2009). Common depth of slab-mantle decoupling: Reconciling
331 diversity and uniformity of subduction zones. *Geochemistry, Geophysics, Geosystems*,
332 10(10).
- 333 Wilkinson, M. D., Dumontier, M., Aalbersberg, Ij. J., Appleton, G., Axton, M., Baak,
334 A., et al. (2016). The FAIR guiding principles for scientific data management and
335 stewardship. *Scientific Data*, 3(1), 1–9.